Journal of Nano- and Electronic Physics
Vol. **10** No 6, 06038(13pp) (2018)

Журнал нано- та електронної фізики
Том **10** № 6, 06038(13cc) (2018)

Influence of UV Light of Extraterrestrial Solar Irradiance on Structure and Properties of ZnO Films Prepared Through Pulsed Electrochemical Deposition and via SILAR Method

N.P. Klochko[1], K.S. Klepikova[1,*], S.I. Petrushenko[2], V.R. Kopach[1], G.S. Khrypunov[1], D.O. Zhadan[1], S.V. Dukarov[2], V.M. Lyubov[1], M.V. Kirichenko[1], S.V. Surovitskiy[1], A.L. Khrypunova[1]

[1] *National Technical University "Kharkiv Polytechnic Institute", 2, Kyrpychov Str., 61002 Kharkiv, Ukraine*
[2] *V.N. Karazin Kharkiv National University, 4, Svobody Square, 61022 Kharkiv, Ukraine*

(Received 29 August 2018; revised manuscript received 29 November 2018; published online 18 December 2018)

The investigations of effect of long-wave (UVA) and short-wave (UVC) ultraviolet light of extraterrestrial solar irradiance on the nanostructured zinc oxide arrays, which were grown by pulsed electrodeposition, as well as on the ZnO and ZnO:In films produced by Successive Ionic Layer Adsorption and Reaction technique (SILAR) confirmed their suitability as UVA-active photosensitive materials. The crystal structure, surface morphology, chemical composition and optical properties found no obvious significant destructive changes after UVC irradiation. However, we detected some irreversible changes in the nature of point defects under the influence of UVC, which affect the ZnO and ZnO:In resistivity, activation energy, photosensitivity and thermoelectrical properties.

Keywords: Extraterrestrial UV light, Zinc oxide, ZnO:In, Pulse electrodeposition, SILAR, Point defect.

DOI: 10.21272/jnep.10(6).06038 PACS numbers: 61.46.Km, 68.37.Ps

1. INTRODUCTION

Sunlight in space at the top of Earth's atmosphere, which is named as extraterrestrial solar irradiance, contains of about 10 % of ultraviolet light (UV) with a wide range of wavelengths (λ), mostly with $\lambda = 100$-399 nm, having total UV intensity of about 140 W/m^2. Therefore, the influence of solar UV on the different materials and its impact on the environment as a whole is very important and is widely researched [1-10]. In particular, an effect of long-wave (315-399 nm) ultraviolet A (UVA), which is not absorbed by the ozone layer and is arrived the earth's surface, is studied in detail for ground applications [2-9]. A short-wave (100-279 nm) ultraviolet C (UVC) is completely absorbed by the ozone layer and atmosphere, and this ultraviolet part of the solar spectrum drives the photochemistry of a number of considerable atmospheric trace gases such as ozone, nitrogen dioxide and hydroxyl radicals and thus has significant effect on the terrestrial and aquatic ecosystems [1, 2]. Influence of UVC on organic plastics and different inorganic materials is manifested in photochemical reactions which lead to the photodegradation [2-3]. Apart from this, in the terrestrial conditions, the small wavelengths or high energies of UV have application depending on the specific discipline in fluorescence diagnostics, germicidal equipment, corneal surgery, high-energy astronomy and physics, gas species detection, lithography of circuits, and in laser optics.

Appropriate thin film coatings for the spectral region shorter than the visible range (UV-active materials) require special considerations with regard to layers insensitive to ultraviolet. Among them, wide-band gap semiconductor zinc oxide (ZnO) ($E_g = 3.37$ eV) is one of the most important UV-active materials. The ZnO nanostructures and thin films are employed as stable components of nanocomposites for the UV-protection of different coatings [4], in sunscreens as inorganic physical blockers for the UV radiation, in UV-filters and as photocatalysts [4-5], in UV-photodetectors and semi-transparent UV-active solar cells [6-9]. In recent years, many studies have been devoted to the efficient photocatalytic decomposition of microbes and organic pollutants of water resources using ZnO nanostructures under UVC irradiation [10-11]. However, we were not able to find in the literature information about the UVC effect on the nanostructured material ZnO itself.

There is a huge amount of various techniques for the nanostructured zinc oxide material obtaining. Among other methods, low temperature aqueous solution growth of doped and non-alloyed ZnO films, for example, through the electrochemical deposition or Successive Ionic Layer Adsorption and Reaction technique (SILAR), become very popular in recent years [5-8, 7-9] because they allow to deposit these materials over large areas and suggest low capital expenditure based on simple process equipment. In [11] we have shown effect of UVA irradiation ($\lambda = 315$-399 nm) on the wettability of the pulsed electrodeposited one-dimensional (1-D) ZnO nanostructures. The investigation [11] represents the electrodeposited in the pulsed mode 1-D ZnO nanostructure array as an adaptive material, which can be reversibly transformed from the mode of high hydrophobicity to hydrophilicity upon exposure to UVA radiation, and then return to the initial wettability state upon storage in the dark. In [9] the photosensitivity towards UVA (370 nm $\geq \lambda \geq$ 365 nm) of the 1-D ZnO nanostructure arrays electrodeposited in the pulsed mode were tested and verified by their dark and light current-voltage characteristics, capacity-voltage characteristics and temporal response curves under the influence of UVA part of sunlight. Analysis of the electronic and electrical parameters of

* catherinakle@gmail.com

the ZnO arrays has shown an important role of the high double Schottky barriers created at the ZnO intergrain boundaries and allowed us to determine the conditions for the obtaining of 1-D ZnO arrays with enhanced and stable photosensitivity towards UVA and the excellent output parameters of the developed on their base test sample of the UVA photosensor of a new generation. However, the influence of the short-wave ultraviolet part of the extraterrestrial solar radiation, especially of the UVC, on structure and properties of these 1-D ZnO arrays has not been studied.

In this work we investigate the effect of the UVC radiation on crystal structure, optical and electrical properties of the nanostructured zinc oxide arrays, which were grown by pulsed electrodeposition, as well as of ZnO and indium doped ZnO:In films produced by the SILAR method. Since the photosensitivity of the semiconductor materials is directly related to their band structure, including those with defect levels in the band gap [8], the influence of UVC on the thermal activation energy of electrical conduction (E_a), on thermoelectric characteristics and on the photosensitivity range of the ZnO and ZnO:In films is analyzed.

2. EXPERIMENTAL DETAILS

Nanostructured 1-D ZnO arrays were obtained by cathodic electrochemical deposition using a standard thermostatic three-electrode electrochemical cell with platinum spring as counter-electrode and saturated Ag/AgCl reference electrode in unstirred aqueous electrolyte containing 0.01 M $Zn(NO_3)_2$ and 0.1 M $NaNO_3$ on SnO_2:F/glass (FTO, TEC 7 Pilkington Company, USA) substrates with 1.5×2 cm^2 area. Temperature of the electrolyte was 70 °C. Firstly, ZnO seed layers were formed via potentiostatic electrochemical deposition provided by a programmable impulse potentiostat PI-0.5-1.1 during short time (30 s) at potential $U = -1.3$ V (here and below, vs. Ag/AgCl). After that, a plating of 1-D ZnO was carried out in the same electrolyte during 15 or 30 min in the pulsed mode by applying rectangular potential pulses. The lower and upper potential limits were, respectively, $U_{off} = -0.7$ V and $U_{on} = -1.3$ V. A duty cycle ($D_c = 0.4$) was given as relation $T_{on}/(T_{on} + T_{off})$, where T_{on} is a time at potential U_{on}, and T_{off} is a time at potential U_{off}. Potential pulse frequency f was 2 Hz. As a result, 1-D ZnO arrays with average thickness (t), which corresponds to the length of nanorods, $t \approx 0.9$ μm and $t \approx 1.1$ μm, respectively, were grown on FTO surfaces.

Depositions by means SILAR method of undoped and indium-doped zinc oxide films, ZnO and ZnO:In, respectively, on glass substrates with 1.0×2.5 cm^2 area were carried out using 120 or 185 mM potassium zincate (K_2ZnO_2) aqueous solutions as cationic precursors and hot water bath as anionic precursor. Cationic precursors were aqueous solutions contained 120 or 185 mM ZnO and 2.7 M KOH. For a deposition of ZnO:In films, the cationic precursor composition included additionally 9 mM of indium chloride ($InCl_3$). One SILAR growth cycle consists of following three steps: (1) immersing the substrate into cationic precursor for 2 s; (2) immersing this substrate immediately into anionic precursor, namely into hot (90 °C) water for 2 s to form ZnO (or ZnO:In) monolayer; (3) rinsing the substrate in a separate H_2O beaker for 5 s to remove loosely bound particles. By repeating such deposition cycles for 200 or 400 times, we obtained ZnO (or ZnO:In) films, which thickness t (t in the 2.0-2.2 μm range) was determined gravimetrically, taking for a calculation the bulk ZnO density 5.61 g/cm^3. After the deposition via SILAR, the unnecessary ZnO and ZnO:In layers from the opposing sides of the substrates were removed by a rubbing with a dilute sulfuric acid (20 % H_2SO_4). Then, ZnO and ZnO:In film samples were annealed at 200 °C for 1 h in vacuum.

Irradiation by the UVC of the electrodeposited 1-D ZnO arrays and of the obtained via SILAR method ZnO and ZnO:In film samples was carried out using a barrier discharge lamp with argon filling having maximum energy illumination in the plane of the lamp window ~ 10^{20}-10^{21} quantum/m^2 with a maximum energy 10.5 eV ($\lambda \geq 118$ nm). The irradiated samples were densely pressed to the lamp window. The UVC irradiation was carried out in air at $T = 300$ K for 10 hours.

Morphology of the films was observed by scanning electron microscopy (SEM) in a secondary electron mode. The SEM instrument "Tescan Vega 3 LMH" was operated at an accelerating voltage 30 kV without the use of additional conductive coatings.

Elemental analysis of the samples was carried out by X-ray fluorescence (XRF) microanalysis using an energy dispersive spectrometry (EDS) system "Bruker XFlash 5010". Energy dispersion spectra were taken from the 50×50 μm sample areas. Quantification of the spectra was carried out in the self-calibrating detector mode. Note that Si as the main component of glass substrates was excluded from the quantification.

Optical properties of ZnO and ZnO:In layers were studied in the wavelength range 300-1100 nm, both before and after vacuum annealing with an "SF-2000" spectrophotometer equipped with "SFO-2000" reflection attachment for a registration of diffuse reflection spectra $R_d = f(\lambda)$. Glass substrates or FTO substrates were used as control samples when optical transmission spectra $T_o(\lambda)$ were recorded for the deposited via SILAR ZnO and ZnO:In films or for the electrodeposited 1-D ZnO arrays, respectively. Optical band gaps E_g of the films were determined from their absorption coefficients (α) calculated as described in [12]:

$$\alpha = 1/t \times \ln(1/T_0) \quad (1)$$

Then, the optical bandgaps E_g were obtained via the following equation [12]:

$$(\alpha \cdot h\nu)^2 = A \cdot (h\nu - E_g), \quad (2)$$

where A is a constant and hν denotes the photon energy. The E_g value has been obtained graphically through an extrapolation of the linear portion of the $(\alpha \cdot h\nu)^2$ dependence on $h\nu$.

The Urbach energy (E_0), which originates from the optical transitions assisted by sub-bandgap photons due to availability of a large number of point defects in the forbidden band was determined, in accordance with [13], by equation:

$$\alpha = \alpha_0 \cdot \exp\left(h\nu / E\right), \quad (3)$$

where α_0 is a constant.

According to [13], the structural disorder of the film was assessed from the E_0 determined by fitting the linear portions of $\ln(\alpha)$ versus $h\nu$, namely, from the slope of the linear part of the dependence $\ln(\alpha)$ on $h\nu$ near the band gap energy value.

The photoluminescence (PL) spectra were obtained on the spectrometer LabRam HR800 in the backscattering geometry at room temperature. Excitation was carried out using the Ar^+ laser with frequency doubling (excitation line 244 nm, excitation density 10^{21} photon/(s·cm^2), incident radiation power ~ 2.5 mW). Lens with 40 × magnification was used for laser radiation focusing; laser spot diameter on the sample was 3-4 μm.

To analyze phase compositions, structural and substructural parameters of ZnO and ZnO:In layers, we recorded X-ray diffraction (XRD) patterns by a "DRON-4" diffractometer. Scanning was performed with Bragg-Brentano focusing (theta – 2 theta). The resulting XRD patterns were processed and the profile parameters of the diffraction lines were calculated by "New-Profile v.3.4 (486)" and "OriginPro v.7.5" software. The presence of crystalline phases was revealed by comparing the experimental diffraction patterns with the reference database JCPDS by using PCPDFWIN v.1.30 software. In accordance with [14], to evaluate crystallite size D and lattice microstrains induced mainly by point defects $\varepsilon = \Delta d/d$ (where d is the crystal interplanar spacing according to JCPDS, and Δd is the difference between the corresponding experimental and reference interplanar spacings) we applied the X-ray line broadening method using the Scherrer equation and the Williamson-Hall approximation. The crystal lattice constants, a and c, of the nanocrystalline ZnO or ZnO:In grains were calculated from the positions of the pairs of adjacent to each other indexed lines in the X-ray diffraction patterns by the Nelson-Reilly graphical extrapolation method and refined using the least-squares method (LSM) by UnitCell software on the basis of all recorded reflections in the X-ray diffraction patterns, as in [9]. Texture quality of ZnO and ZnO:In layers was estimated by the Harris method [7, 9]. Pole density P_i, which determines an axis of the crystal plane that is oriented normal to the surface, was calculated according to the equation [7, 9]:

$$P_i = \left(I_i / I_{0i}\right) / \left(1/N \sum_{i=1}^{N} \left(I_i / I_{0i}\right)\right), \quad (4)$$

where I_i, I_{0i} are integral intensity of the i-th diffraction peak of the film and etalon, respectively; N is the number of lines presented in the diffraction. Texture axis has the index, which corresponds to the largest value of P_i. The orientation factor f for the relevant direction was calculated from the formula [7]:

$$f = \sqrt{1/N \sum_{i=1}^{N} (P_i - 1)^2}. \quad (5)$$

The resistivities ρ of ZnO and ZnO:In films on glass substrates were measured at temperatures T in the 300-325 K range by using a four-point collinear probe resistivity method in accordance with [15]. The resistivity was calculated according to [15] as follows:

$$\rho = \left(\pi t \delta U_{23}\right) / \left(I_{14} \ln(2)\right), \quad (6)$$

where U_{23} is the voltage between the second and third probe; I_{14} is the current between the first and fourth probes; δ is a correction factor for the accounting the ratio of the distance between the probes and the size of the film; $\pi\delta/\ln(2) \approx 4.45$.

The thermal activation energy of electrical conductivity $\sigma = \rho^{-1}$ for ZnO and ZnO:In films E_a was calculated in accordance with [16, 17] by using equation:

$$\sigma = \sigma_0 \cdot \exp\left(-E_a / kT\right), \quad (7)$$

where σ_0 is a parameter depending on the characteristics of thin film samples and k denotes Boltzmann's constant. In accordance with proposed in [17], for the determination of E_a of the deposited via SILAR ZnO and ZnO:In films on glass substrates we used dependences $\ln R = f(10^3/T)$ in the temperature range 300-325 K, applying the resistances R between two adjacent ohmic aluminum banded contacts in the Al/ZnO/Al and Al/(ZnO:In)/Al test samples shown in Fig. 1(a). These Al contacts were deposited in vacuum and have 1.0 × 0.2 cm^2 area each with a distance between the neighboring contacts ~ 0.2 cm.

Electrical properties of the electrodeposited zinc oxide nanorods in 1-D ZnO arrays were analyzed by using Al/FTO/ZnO/Al test samples presented in Fig. 1(b) with Al band contacts, which vacuum deposition was performed at 70° angle from the normal to the FTO/ZnO plane through a shadow mask to prevent short circuits in the separate locations of the ZnO and FTO areas. Data on the electrical conductivity σ of the zinc oxide nanorods were obtained from the dark current-voltage (I-V) characteristics, as detailed in [9]. The thermal activation energy E_a for electrical conductivity of 1-D ZnO was calculated by using expression (7) and dependence $\lg I$ measured at constant V value versus $10^3/T$ for Al/FTO/ZnO/Al test sample shown in Fig. 1(b) during its cooling in air in the temperature interval from T = 325 K to T = 300 K.

A conductivity type of the 1-D ZnO arrays was determined using a standard hot-probe method. To assess the conductivity type of ZnO and ZnO:In thin films, the in-plane Seebeck coefficients Z at the temperature range 293-315 K were measured using a homemade installation described in [7] as thermoelectric voltages induced in response to the temperature gradients ΔT along the films deposited on glass substrates, when the distance between hot and cold probes in the form of gold rings was 2.3 cm. Then, the thermoelectric power factors P for ZnO and ZnO:In films were calculated as Z^2/ρ.

Light and dark I-V characteristics (and J-V characteristics, where $J = I/S_l$ is the current density and S_l is the area of the ZnO or ZnO:In cross-sectional area through which the current flows, that is determined by the geometry of the contacts in the test samples in Fig. 1) and also temporal response curves under the influence of UVA and visible light were measured as described in [9] for the deposited via SILAR ZnO and

ZnO:In films on glass substrates by using of Al/ZnO/Al and Al/(ZnO:In)/Al test samples (Fig. 1(a)) and for the electrodeposited 1-D ZnO arrays by applying Al/FTO/ZnO/Al test samples shown in Fig. 1(b). The dark *I-V* characteristics were detected by the amperemeter-voltmeter technique described in detail in [7]. To measure light *I-V* characteristics and photoresponse curves, the test samples were illuminated with UVA ($\lambda = 365$ nm), violet ($\lambda = 410$ nm), blue ($\lambda = 465$ nm), green ($\lambda = 525$ nm) or red ($\lambda = 625$ nm) light-emitting diodes having wide-angle beam divergences to ensure uniform illumination from the glass side. The intensity (power density) of the light on the test sample surface was 0.05 W/cm^2 or 0.5 W/cm^2. Photocurrent I_{ph} was recorded during $\tau_{UV} = 300$ s, after that, the light was turned off. The I_{ph} was measured at bias voltage 1.0 V. The photocurrent density calculated, taking into account the dark current I_{dark} at bias voltage 1.0 V, as $J_{ph} = (I_{ph} - I_{dark})/S_l$. For the deposited via SILAR ZnO and ZnO:In films $S_l \approx (2.0\text{-}2.2)\cdot 10^{-4}$ cm^2, and for the electrodeposited 1-D ZnO arrays $S_l \approx 0.06$ cm^2. A photosensitivity S of ZnO and ZnO:In films, and also of the electrodeposited ZnO nanorods was calculated as $S = J_{ph}/J_{dark}$, where J_{dark} is current density in dark at bias voltage 1.0 V. In accordance with [18], the photoresponse time τ_p of the test samples was determined as the time required to achieve 63 % of the maximum photocurrent I_{ph} after the start of the optical effects of light. The reset time τ_r was defined, according to [18], as the elapsed time to reach the 37 % of the maximum photocurrent from the switching off the optical light. A multiple repeated "on-off" switching of the irradiation was used to confirm the reproducibility and stability of the test sample work.

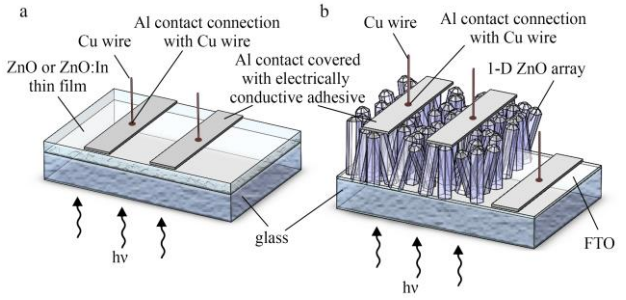

Fig. 1 – Schematic illustration of the test samples with deposited via SILAR on glass substrates ZnO and ZnO:In thin films (a) and with electrodeposited on FTO substrate 1-D ZnO array (b)

3. RESULTS AND DISCUSSIONS

Fig. 2 demonstrates SEM images (a, b), X-ray diffraction patterns (c) and optical properties (d) of the 1-D ZnO nanostructured arrays electrodeposited in the pulsed mode. It can be seen in Fig. 2(a) that the sample, which was electrodeposited within 30 min, consists of thicker (~ 400 nm in diameter) and longer ($t = 1.1$ μm) nanorods. The average diameter of the nanorods of the sample in Fig. 2(b), which was electrodeposited for twice less time (15 min), is ~ 200 nm, these nanorods look shorter, the measurements gave value $t = 0.9$ μm. There are no obvious signs of destructive influence of the UVC, i.e. no trace of photo-corrosion on the nanorods in the electrodeposited 1-D ZnO array in Fig. 2(b).

Analysis of XRD patterns in Fig. 2(c) has shown that all electrodeposited 1-D ZnO arrays are single-phased, polycrystalline in nature and matching with hexagonal wurtzite structure ZnO (JCPDS 36-1451). As calculations of structural parameters have revealed (Table 1), ZnO only very little and not always is preferentially oriented along the characteristic for the 1-D ZnO nanostructures <001> direction (the orientation factor in the (002) plane $f \leq 0.6$ a. u.), that can be explained by the short length of the nanorods. Calculations of the 1-D ZnO crystallite size via the Williamson-Hall approximations for the samples with $t = 1.1$ μm, and using the Scherrer equation for 1-D ZnO with $t = 0.9$ μm have shown, that the observed decrease in D due to the influence of the UVC is within the error of the experiment. Nevertheless, after UVC irradiation of the 1-D ZnO arrays, we can observe the increase of the microstrains ε that is evidently related to the crystal lattice parameters, a and c, which after UVC irradiation exceed the reference data JCPDS 36-1451 noticeably. The data on optical studies of these samples show (Fig. 2(d)) that the transmittance of ZnO layers naturally decreases, and the reflectance of a predominantly diffuse nature grows with their thickness, which is typical for nanostructures. Studies of effect of the UVC on optical properties of the electrodeposited 1-D ZnO arrays found no destructive changes. The band gap E_g of these samples is close to those characteristic of bulk zinc oxide both before and after UVC irradiation, and the smaller values of the band gap are observed (Fig. 2(d)) for the samples with longer nanorods irrespective of the UVC. The 1-D ZnO arrays with $t = 1.1$ μm have rather high Urbach energies (E_0 are 0.70 and 0.56 eV before and after UVC irradiation, respectively), indicating the presence of large number of trap states, the formation of which is induced by intrinsic defects produced unintendedly during deposition. In general, according to [19], our studies of E_g and E_0 have shown a tendency to reduce the number of defects in 1-D ZnO arrays after UVC irradiation. Probably, an explanation for the observed is a change in the nature of point defects under the influence of UVC, which creates an impression that the XRD data and the optical studies of the electrodeposited 1-D ZnO arrays concerning contradict each other.

Results of the study of ZnO and ZnO:In films deposited on glass substrates via SILAR using 120 mM ZnO in the cationic precursor solution before UVC irradiation are shown in Fig. 3. Comparison of its SEM images in Fig. 3(a) and Fig. 3(b) reveals the effect of indium chloride in the cation precursor on the film morphology. Chemical X-ray fluorescence microanalysis (Fig. 3(c)) has displayed, that ZnO:In films, both as-deposited and annealed in vacuum at 200 °C for 1 h, contain Zn, O and ~ 1 at.% In. Besides of these basic elements, X-ray fluorescence spectrum of the as-prepared via SILAR ZnO:In film contains carbon associated with CO_2 adsorbed on the surface from air. Analysis of X-ray diffraction patterns (Fig. 3(d)) reveals that ZnO and ZnO:In films after their vacuum annealing are single-phased, polycrystalline and have the wurtzite hexagonal ZnO structure (according to JCPDS #36-1451).

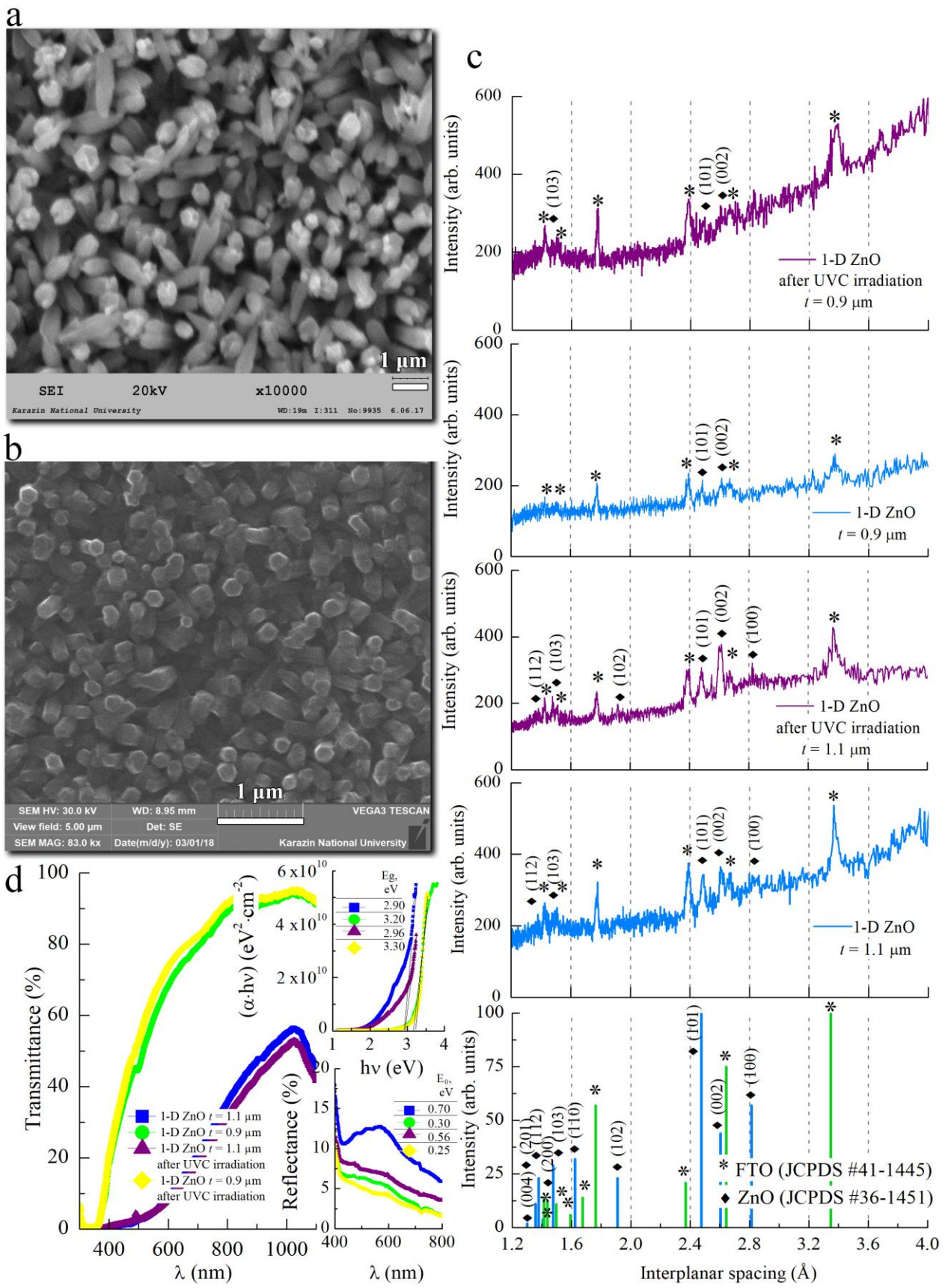

Fig. 2 – Top view SEM images of the electrodeposited 1-D ZnO arrays as-prepared (t = 1.1 μm) (a) and irradiated by the UVC (t = 0.9 μm) (b). (c) – XRD patterns of the electrodeposited 1-D ZnO arrays before and after irradiation by the UVC. (d) – Optical properties of these electrodeposited 1-D ZnO arrays

Since no extraneous peaks were detected in the XRD of indium-doped zinc oxide films, it is possible to assume the formation of the solid solutions for ZnO:In films before and after vacuum annealing. Calculations of crystallite sizes D by the Williamson-Hall approximations using the broadening of X-ray diffraction peaks, that are shown in Table 2, testify that the doping of zinc oxide by indium slightly reduces grain size (from D = 38 nm for ZnO to D = 30 nm for ZnO:In) and increases microstrains ε (from $3.4 \cdot 10^{-3}$ to $4.6 \cdot 10^{-3}$ a. u., respectively). The crystal lattice constants a of these ZnO and ZnO:In films are approximately the same as the reference ZnO according to JCPDS #36-1451, but the c value of the ZnO:In film is increased by 0.4 %. Probably, the deformation of the ZnO:In crystal lattice is caused by the presence of point defects, in particular, indium in the interstitial and substitutional sites, i.e. In_i and In_{Zn}, respectively. As seen in Fig. 3(d) and Table 2, these ZnO and ZnO:In films have a weakly pronounced texture in the (002) plane, which is characteristic for ZnO, however, their orientation factors f do not exceed 0.6 a. u.

Optical properties of the as-deposited via SILAR on glass substrates ZnO and ZnO:In films are presented in Fig. 3(e). It can be seen that both films are translucent in the visible range. Note that vacuum annealing causes no noticeable changes in their optical properties (not shown here). The $T_0(\lambda)$ spectra do not contain any interference extremes, which is well explained by their surface morphology presented in Fig. 3(a, b) and is consistent with their large diffuse reflectance in the entire visible range. The band gap E_g for direct optical transitions in the SILAR deposited ZnO and ZnO:In films $E_g \approx 3.0$-3.1 eV are slightly less than the characteristic for zinc oxide value 3.37 eV, probably, because the Urbach energies of ZnO and ZnO:In films deposited via SILAR are rather large, $E_0 \approx 0.6$ eV, which agree well with their nanocrystalline structure having characteristic surface states and point defects in the crystal lattice.

Fig. 4 demonstrates effect of UVC irradiation on the ZnO:In film deposited on glass substrate via SILAR using 185 mM ZnO in cationic precursor solution. SEM image in Fig. 4(a) shows layer, which consists of small squat ZnO:In nanorods ~ 400 nm in diameter without any traces of photo-corrosion. X-ray fluorescence microanalysis (Fig. 4(b)) has displayed, that UVC-irradiated ZnO:In film contains Zn, O, In, and also K and Ca from the glass substrate. The lack of carbon in the XRF spectrum is explained by the desorption of CO_2 from the ZnO:In surface as a result of UVC irradiation. As it seen in inset in Fig. 4(c) and in Table 2, UVC irradiation with vacuum annealing of this ZnO:In film promotes a reduction of the ZnO:In crystal lattice to values characteristic of zinc oxide, while maintaining $D \approx 30$ nm and a high level of microstrains, which, in our opinion, is evidence of a modification of defects and/or a decrease in their number in the film structure after UVC treatment with vacuum annealing. According to the results of the optical analysis (Fig. 4(d)), this ZnO:In film after UVC irradiation has the wider bandgap that is close to the characteristic for zinc oxide value ($E_g \approx 3.2$ eV compared with pre-irradiation $E_g \approx 3.0$ eV), and it is characterized by a lower Urbach energy ($E_0 \approx 0.23$ eV compared with pre-irradiation $E_0 \approx 0.47$ eV). Thus, according to the data in Figs. 2-4 and Tables 1-2, in the obtained by the SILAR method ZnO and ZnO:In films, as in the electrodeposited 1-D ZnO arrays, UVC irradiation with energy up to 10.5 eV ($\lambda \geq 118$ nm) does not cause the photo-corrosion, but provides the reconstruction of the surface states and also alters the point defects inside the crystal lattice. As it seen in Fig. 4(d), after UVC irradiation and following vacuum annealing $E_g \approx 3.1$ eV, $E_0 \approx 0.55$ eV, probably, because of the appearance of new defect states in the ZnO:In film.

The electrodeposited zinc oxide layers have n-type conductivity. In the dark, the resistivity ρ of the 1-D ZnO arrays was ~ 10^4 Ω·cm. Analysis of the temperature dependence of the conductivity σ of the 1-D ZnO array (t = 1.1 μm), which SEM image is presented in Fig. 2(a), has revealed (Fig. 5(a)) a decrease in the activation energy from E_a = 0.14 eV to E_a = 0.06 eV as the sample was cooled from 325 to 300 K. According to [19-21], both these small activation energies can correspond to such shallow point defects as neutral and doubly charged zinc interstitials (Zn_i and Zn_i^{++}), neutral and singly charged oxygen vacancies (V_O^o and V_O^+) and

Table 1 – Structural parameters of the pulsed electrodeposited 1-D ZnO arrays on FTO substrates

1-D ZnO array thickness t, μm	Crystallite size D, nm	Microstrains ε, 10^{-3} a. u.	Lattice parameters, Å				Texture		
			Nelson-Reilly method		LSM		*hkl*	P_{hkil}	Orientation factor f
			a	c	a	c			
Etalon ZnO (JCPDS 36-1451)	–	–	3.249	5.206	3.249	5.206	–	–	–
t = 0.9, as-deposited	27	5	–	–	–	–	–	–	–
t = 0.9, UVC irradiated	7	20	–	–	–	–	–	–	–
t = 1.1, as-deposited	35-100	1.1-2.5	3.255	5.201	3.241	5.224	(100) (102) (112)	1.3 1.5 1.3	0.4
t = 1.1, UVC irradiated	30-120	2.4-4.3	3.268	5.193	3.268	5.213	(002) (100)	2.3 1.2	0.6

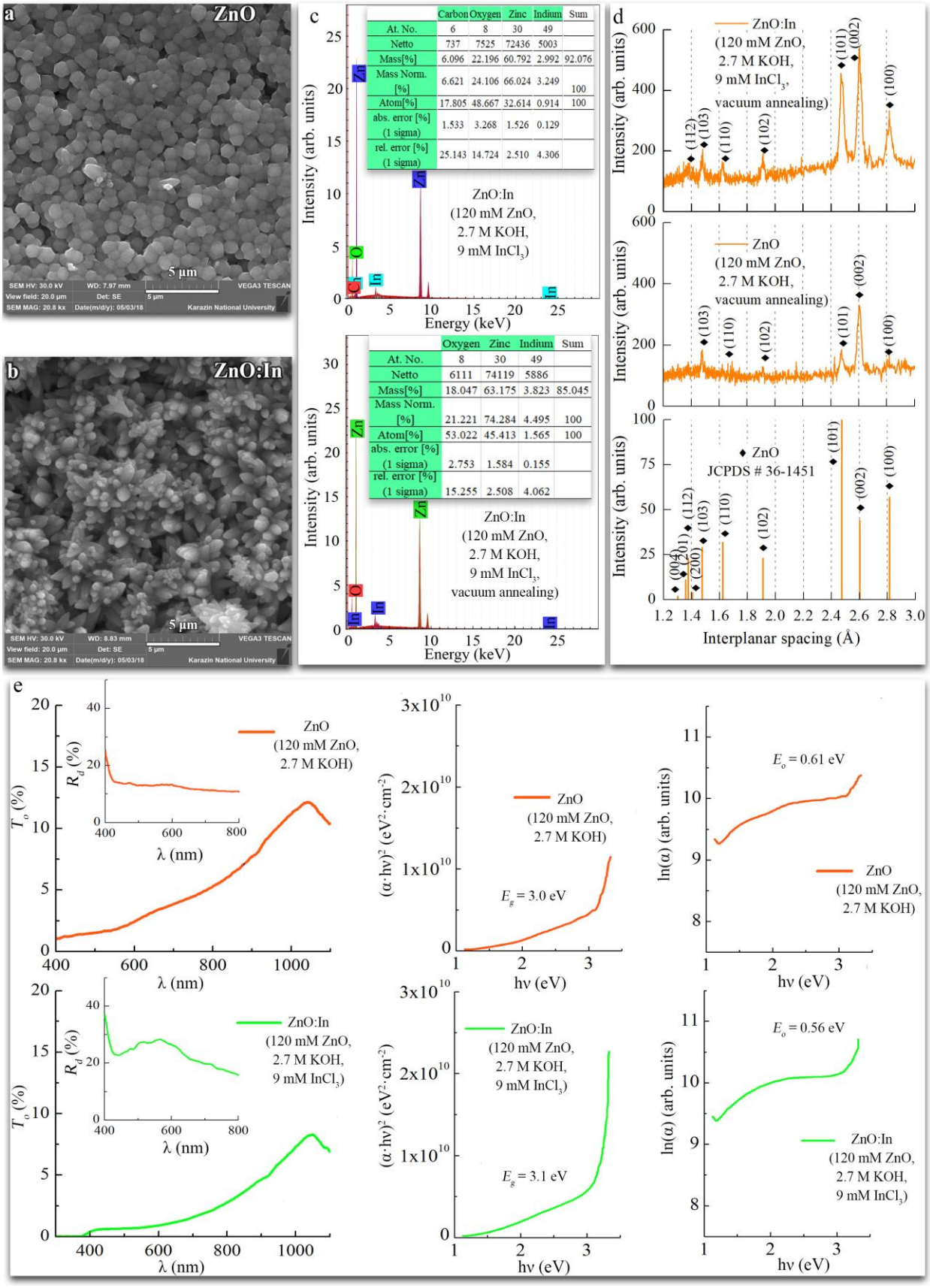

Fig. 3 – Top view SEM images of ZnO (a) and ZnO:In (b) films deposited on glass substrates via SILAR using 120 mM ZnO in cationic precursor solution. (c) – X-ray fluorescence spectra of the said ZnO:In film before and after vacuum annealing. (d) – XRD patterns of these ZnO and ZnO:In films after vacuum annealing. (e) – Optical properties of these films as-prepared

Table 2 – Structural parameters of the ZnO and ZnO:In films obtained via SILAR on glass substrates

Film sample	Cationic precursor	Crystallite size D, nm	Microstrains ε, 10^{-3} a. u.	Lattice parameters, Å				Texture		
				Nelson-Reilly method		LSM		hkl	P_{hkil}	Orientation factor f, a. u.
				a	c	a	c			
Etalon ZnO (JCPDS 36-1451)	–	–	–	3.249	5.206	3.249	5.206	–	–	–
t = 2.0 μm, ZnO vacuum annealed	120 mM ZnO, 2.7 M KOH	38	3.4	3.246	5.203	3.251	5.211	(002)	2.0	0.6
t = 2.1 μm, ZnO:In vacuum annealed	120 mM ZnO, 2.7 M KOH, 9 mM $InCl_3$	29	4.6	3.232	5.236	3.248	5.219	(002)	2.0	0.5
t = 2.2 μm, ZnO:In as-deposited	185 mM ZnO, 2.7 M KOH, 9 mM $InCl_3$	30	3.2	3.245	5.206	3.258	5.204	(002)	3.2	1.0
t = 2.2 μm, ZnO:In vacuum annealed		30	3.2	3.245	5.206	3.258	5.204	(002)	3.2	1.0
t = 2.2 μm, ZnO:In UVC irradiated		30	4.5	3.252	5.211	3.260	5.223	(002)	1.8	0.4
t = 2.2 μm, ZnO:In UVC irradiated and vacuum annealed		27	4.7	3.222	5.233	3.234	5.204	(002)	1.7	0.4

hydrogen interstitials (H_i). Furthermore, it is known [9, 20] that in the nanostructured 1-D ZnO the small length scales and large surface-to-volume ratio mean that surface defects play a strong role in controlling of properties, specifically, the adsorbed gases act as sources and sinks of electrons, and associated space charge regions create excitonic levels in the forbidden band below the conduction band. As shown in [8], if ZnO nanostructures have surface excitonic levels and shallow point defects, which correspond to small E_a, the photoluminescence spectra show near-band emission, for example at 386 nm (3.21 eV) which is associated with excitonic levels and/or zinc interstitials (Zn_i). The PL spectrum in Fig. 5(b) presents intensive UVA emission at ~ 380-390 nm almost without any visible emissions. In accordance with [22-23], such sharp and predominant UVA emission corresponds to the near-band-edge photoluminescence and is derived from the recombination of the free excitons, which demonstrates that the ZnO nanorods have high crystal structure. According to [8, 24-25], the visible PL spectra correspond to deeper defect levels, for example, it is believed in [24] that the recombination of electrons trapped in V_O^+ with photo-excited holes result in the visible emission. According to [24], the visible emission occurs also when the hole trapped at V_O^{++} center recombines with electrons in conduction band. In addition to these possibilities, in accordance with [25], donor-acceptor complex which mostly likely involved oxygen and zinc vacancies can also be responsible for the visible emission.

Light and dark *I-V* characteristics (Fig. 5(c)) and temporal photoresponse curves under the influence of UVA light (λ = 365 nm; power density 0.5 W/cm^2) (Fig. 5(d)) for this electrodeposited 1-D ZnO array by applying Al/FTO/ZnO/Al test sample shown in Fig. 1(b) confirm its photosensitivity to UVA. These data demonstrate that under the influence of long-wave ultraviolet part of sunlight these layers reversibly increase their electrical conductivity. This photoresponse appears as a photoconductivity, which, in turn, is directly related to photoluminescence [8, 25]. It is known [8-9], that the UVA photoresponse of the ZnO nanostructures consists of two parts: a rapid process of photogeneration and recombination of electron-hole pairs, and a slow process of surface adsorption and photodesorption of oxygen molecules. As a demonstration of interconnection of photoluminescence and photoconductivity, some authors [8, 25] show significant visible light photodetection capability of nanostructured ZnO thin films possessing substantially high percentage of oxygen vacancies (neutral *Vo*, singly ionized V_O^+ and doubly charged V_O^{++}) and zinc interstitials (Zn_i, Zn_i^+ and Zn_i^{++}), and also donor-acceptor complexes of oxygen and zinc vacancies. As seen in Fig. 5(e), the electrodeposited 1-D ZnO array is insensitive to visible light, which indirectly confirms the absence of a large number of the above-mentioned deep donor defects Zn_i^+, V_O^+, V_O^{++} and other deep defect states.

High resistance of the as-deposited via SILAR ZnO and ZnO:In films due to the energy surface barriers, which created, according to [8-9, 20, 23], primarily because of the adsorption of oxygen and other atmospheric gases, was reduced to a level that allowed measuring the electric properties by means annealing of ZnO and ZnO:In films in vacuum at 200 °C for 1 h. The obtained ZnO and ZnO:In films have *n*-type conductivity. Fig. 6(a) through the changes of the electrical resistances with temperature of the ZnO and ZnO:In films deposited via SILAR and annealed in vacuum before and after UVC irradiation shows rather small activation energies. ZnO film deposited via SILAR using 120 mM ZnO in cationic precursor solution and then annealed in vacuum has typical for undoped zinc oxide E_a = 0.21 eV (Table 3), which means the presence of native shallow donor point defects (Zn_i, Zn_i^{++}, V_O^o and V_O^+) [8, 16-17, 19-21].

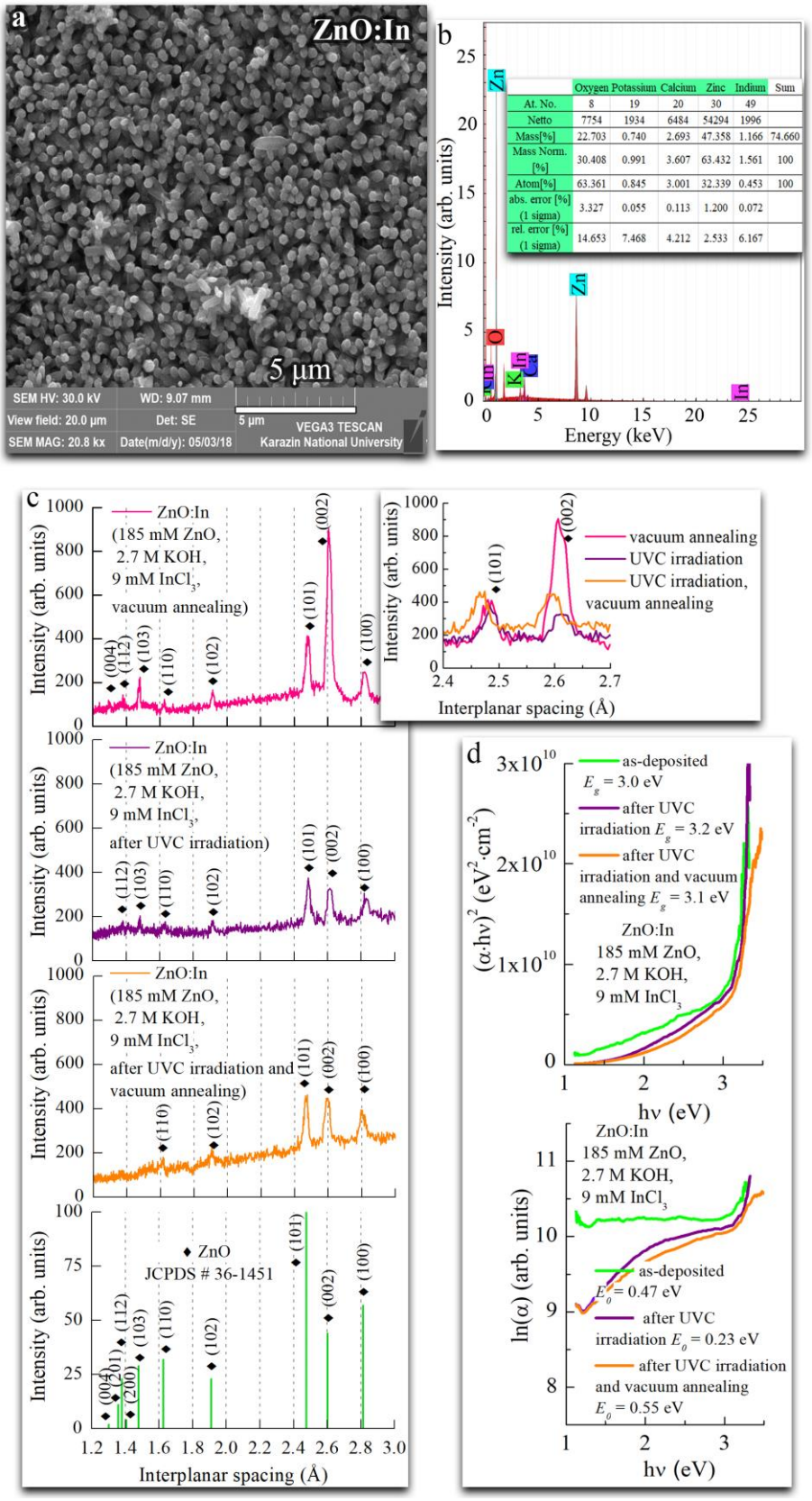

Fig. 4 – (a) – Top view SEM image of ZnO:In film deposited on glass substrate via SILAR using 185 mM ZnO in cationic precursor solution after UVC irradiation and vacuum annealing. (b) – X-ray fluorescence spectra of the said ZnO:In film after UVC irradiation and vacuum annealing. (c) – XRD patterns of ZnO:In films deposited on glass substrate via SILAR using 185 mM ZnO in cationic precursor solution after vacuum annealing, after UVC irradiation and after UVC irradiation with following vacuum annealing. Inset in (c) shows the displacement of two main XRD peaks because of UVC irradiation and vacuum annealing. (d) – Optical properties of these ZnO:In films

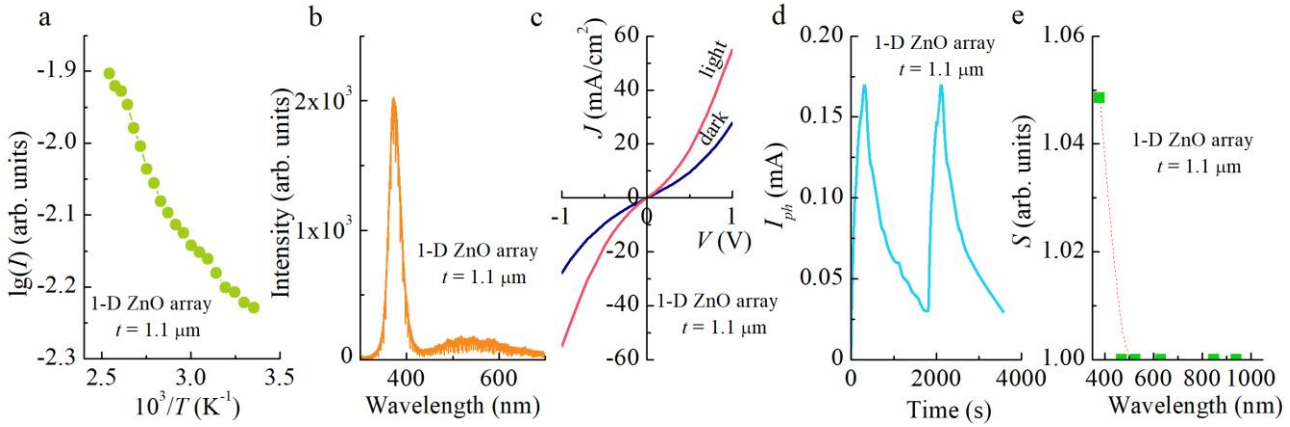

Fig. 5 – Change of the electrical conductivity with temperature through dependence lg$I$ measured at constant V value versus $10^3/T$ (a), PL spectrum (b), dark and light J-V characteristics (λ = 365 nm; power density 0.5 W/cm²) (c), temporal response curve under the influence of UVA light (λ = 365 nm; power density 0.5 W/cm²) (d) and photosensitivity $S = J_{ph}/J_{dark}$ against UVA and visible light (e) of the electrodeposited 1-D ZnO array (t = 1.1 μm)

As it seen in Fig. 6(a) and Table 3, in indium doped ZnO:In films the resistivity is decreased by about 50 times, and the activation energy is reduced by 10 times (E_a = 0.02 eV) compared with undoped zinc oxide, probably due to the appearance of additional shallow donor defects, for example indium interstitial In_i and indium antisite In_{Zn}. The reduced electrical resistivity and activation energy in ZnO:In films prepared by different methods were investigated in literature [17, 26-29], and this phenomenon was explained variously in terms of different lattice defects. Since, similarly to [17, 27] we registered through the XRD data enlarged crystal lattice and the associated microstrains in the annealed in vacuum ZnO:In film (Table 2, Fig. 4(c, inset)), so, the most likely explanation is given in [27-28]. According to [27], the lower resistivity in the film after doping with the optimum indium content can be explained in terms of interstitial indium atom position in the crystal lattice In_i, which behaves as donor. In accordance with [28], indium as substitutional element for Zn can potentially form shallow donors In_{ZnO} in ZnO, which significantly increase the electron concentrations, making the films heavily n-type, but, the larger bond lengths of In-O compared with Zn-O deform the ZnO lattice. As shown in Table 2, Fig. 4(d) and Fig. 5(c, inset), both as-deposited via SILAR and the annealed in vacuum ZnO:In films, and also unannealed ZnO:In film irradiated with UVC, all have enlarged crystal lattice over against ZnO.

Table 3 – Electrical properties of the ZnO and ZnO:In films produced by the SILAR method both before and after UVC irradiation

Sample	SILAR mode		Electrical, photosensitive and thermoelectric properties						
	Cationic precursor	Film thickness t, μm	Average resistivity ρ, Ω·m	Activation energy E_a, eV	Photosensitivity against UVA (λ = 365 nm, power density 0.5 W/cm²)			Seebeck coefficient Z, μV/K	Thermoelectric power factor $P = Z^2/\rho$, μW/(m·K²)
					$S = J_{ph}/J_{dark}$	photo response time τ_p, min	reset time τ_r, min		
ZnO vacuum annealed	120 mM ZnO, 2.7 M KOH	2.0	$98 \cdot 10^{-3}$	0.21	40	6.5	36.7	– 200	0.4
ZnO:In vacuum annealed	120 mM ZnO, 2.7 M KOH, 9 mM $InCl_3$	2.1	$2 \cdot 10^{-3}$	0.02	25	6.5	5.0	– 120	9.0
ZnO:In vacuum annealed and UVC irradiated	185 mM ZnO, 2.7 M KOH, 9 mM $InCl_3$	2.2	$50 \cdot 10^{-3}$	0.22	65	6.5	3.3	– 250	1.3

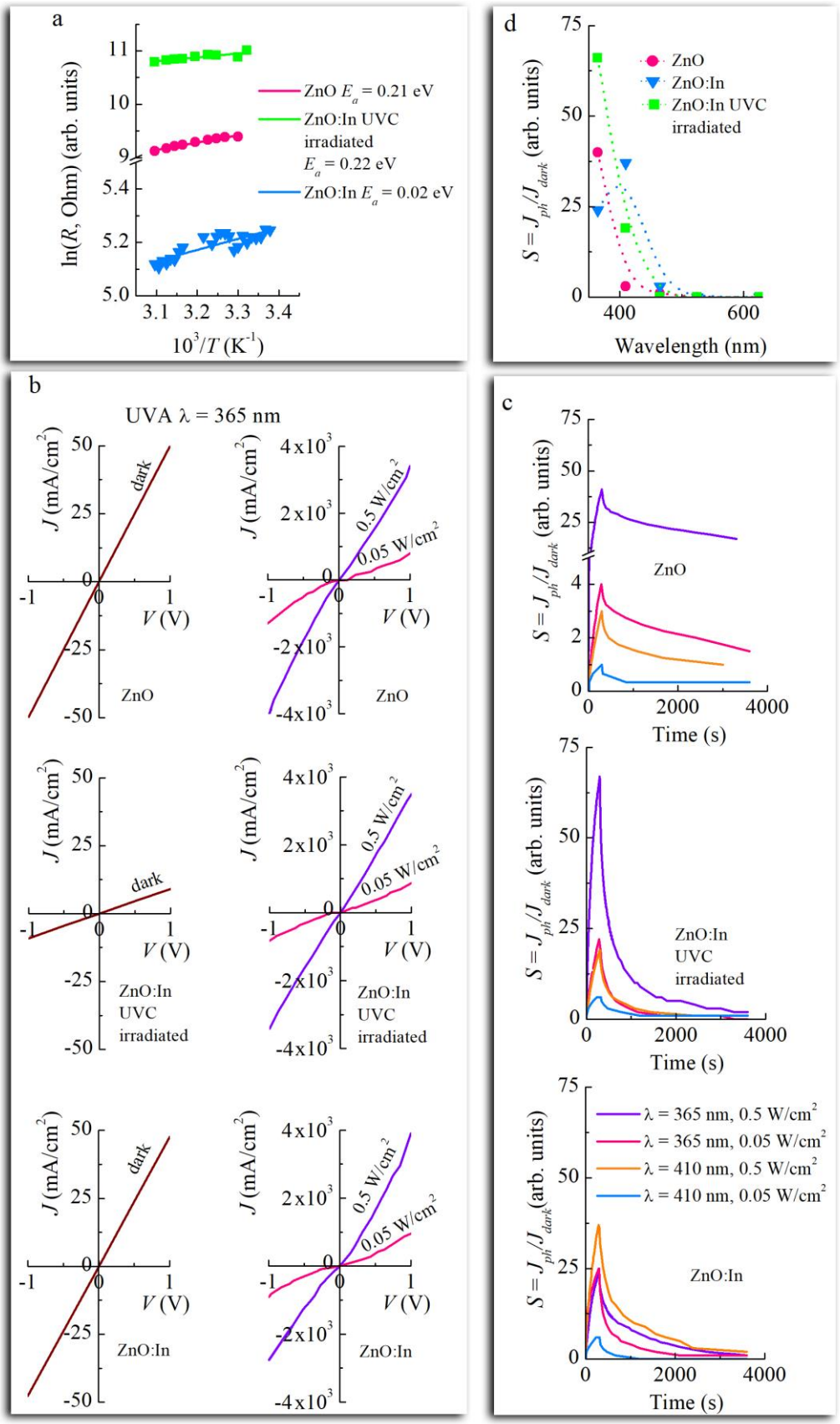

Fig. 6 – Change of the electrical resistance with temperature (a), dark (left) and light (right) *J-V* characteristics ($\lambda = 365$ nm; power densities 0.05 W/cm² and 0.5 W/cm²) (b), temporal response curves under the influence of UVA ($\lambda = 365$ nm) and violet ($\lambda = 410$ nm) light with power densities 0.05 W/cm² and 0.5 W/cm² (c) and photosensitivity $S = J_{ph}/J_{dark}$ against UVA and visible light (d) of ZnO and ZnO:In films deposited on glass substrates via SILAR and annealed in vacuum before and after UVC irradiation

At the same time, our studies found that if the deposited by the SILAR method ZnO:In film was UVC irradiated and then annealed in vacuum at 200 °C for 1 h, its crystal lattice was compressed (Table 2, Fig. 5(c, inset)), the resistivity and activation energy (E_a = 0.22 eV) were appreciated above the level characteristic of the ZnO film (Table 3), which may be an evidence of a reduction in the number of defects in the ZnO:In crystal lattice.

Dark and light *J-V* characteristics (λ = 365 nm; power densities 0.05 W/cm^2 and 0.5 W/cm^2) (Fig. 6(b)) and temporal response curves under the influence of UVA (λ = 365 nm) and violet (λ = 410 nm) light with power densities 0.05 W/cm^2 and 0.5 W/cm^2 (Fig. 6(c)) demonstrate high photosensitivity of the deposited via SILAR ZnO and ZnO:In films after their vacuum annealing towards UVA and violet light. As it seen in Fig. 6 and Table 3, the ZnO and ZnO:In films deposited by the SILAR method are several dozen times more photosensitive with respect to UVA, than the electrodeposited 1-D ZnO arrays. The best photosensitivity is possessed by the UVC irradiated ZnO:In film, mainly because the dark electrical resistance of this film is the largest. The photoresponse time τ_p of the films was about the same, but the reset time τ_r was significantly reduced in ZnO:In as a result of zinc oxide doping. The particularly small τ_r value was recorded by us for the ZnO:In sample that was exposed to UVC irradiation, probably because of the change and decrease in the number of point defects in its structure, and also due to the accompanying desorption of gases from ZnO:In intergrain boundaries. In addition, it is seen in Fig. 6(d) that the annealed in vacuum (without UVC-irradiation) ZnO and ZnO:In films are also slightly photosensitive to blue light (λ = 465 nm), and insensitive with respect to green and red light. The observed blue photosensitivity may be caused by defects in the ZnO lattice (singly ionized oxygen vacancies V_O^+ and zinc interstitials (Zn_i, Zn_i^+ and Zn_i^{++})) [8]. According to [27], an additional blue photosensitivity can be attributed to the formation of the impurity band near ZnO conduction band after indium doping, which is formed by indium interstitial In_i and indium antisite In_{Zn} shallow donor defects. In the case when ZnO:In film was irradiated by UVC and then annealed in vacuum, the reduced parameters of the crystal lattice, the decrease in the resistivity, and the increase in the activation energy E_a up to 0.22 eV detected in this work can be explained, to our opinion, as a reduction in the number of shallow donors (their halving) when the zinc interstitials Zn_i, Zn_i^+ and Zn_i^{++} and indium interstitial In_i take the sites of oxygen vacancies V_O^+, thus creating zinc antisite (for instance, ZnO) and indium antisite (perhaps, In_O), respectively. The above-mentioned decrease in the number of defects also explains well the lack of blue photosensitivity for the UVC irradiated and annealed in vacuum ZnO:In film in Fig. 6(d).

Analysis of thermoelectric properties of the ZnO and ZnO:In films produced by the SILAR method and annealed in vacuum shows a decrease of the Seebeck coefficient due to doping with indium and its rise as a result of UVC irradiation (Table 3). According to [30], the Seebeck coefficient growth in the nanostructured zinc oxide films is an evidence of the carrier concentration lessening. Since the concentration of carriers in such objects is determined, on the one hand, by surface adsorption-desorption processes and, on the other hand, by the presence of shallow point donor defects [9, 18, 23], it can be asserted that for the equally annealed in vacuum ZnO:In films, an increase in the Seebeck coefficient for the UVC irradiated sample is an additional evidence of the decrease in the amount of point defects in the film structure due to UVC irradiation. As can be seen in Table 3, both doping ZnO with indium and UVC irradiation of ZnO:In films alter thermoelectric power factors appropriately.

4. CONCLUSIONS

The investigations of effect of UVA and UVC light of extraterrestrial solar irradiance on the nanostructured zinc oxide arrays, which were grown by pulsed electrodeposition, as well as on the ZnO and ZnO:In films produced by the SILAR method confirmed their suitability as UVA-active photosensitive materials. The crystal structure, surface morphology, chemical composition and optical properties found no obvious significant destructive changes after UVC irradiation. However, we detected some irreversible changes in the nature of point defects under the influence of UVC, which affect the ZnO and ZnO:In resistivity, activation energy, photosensitivity and thermoelectrical properties. The effect of the UVC irradiation can be explained as the halving of shallow donors when the zinc interstitials Zn_i, Zn_i^+ and Zn_i^{++} and indium interstitial In_i take the sites of oxygen vacancies V_O^+, thus creating zinc antisite (for instance, ZnO) and indium antisite (perhaps, In_O), respectively.

Conflicts of interests are not available.

Вплив УФ випромінювання позаземної сонячної радіації на структуру і властивості плівок ZnO виготовлених імпульсним електрохімічним осадженням і методом SILAR

Н.П. Клочко[1], К.С. Клепікова[1], С.І. Петрушенко[2], В.Р. Копач[1], Г.С. Хрипунов[1], Д.О. Жадан[1], С.В. Дукаров[2], В.М. Любов[1], М.В. Кіріченко[1], С.В. Суровицький[1], А.Л. Хрипунова[1]

[1] *Національний технічний університет «Харківський політехнічний інститут», вул. Кирпичова, 2, 61002 Харків, Україна*

[2] *Харківський національний університет ім. В.Н. Каразіна, 4, пл. Свободи, 61022 Харків, Україна*

Дослідження впливу довгохвильового (УФА) і короткохвильового (УФС) ультрафіолетового випромінювання позаземної сонячної радіації на наноструктуровані масиви оксиду цинку, які були вирощені імпульсним електроосадженням, а також на плівки ZnO і ZnO:In, виготовлені методом послідовної адсорбції і реакції іонних шарів (SILAR) підтвердили їх придатність в якості УФА-активних фоточутливих матеріалів. Кристалічна структура, морфологія поверхні, хімічний склад і оптичні властивості не виявили явних, значних, деградуючих змін після УФС опромінення. Однак, ми виявили деякі незворотні зміні в природі точкових дефектів під впливом УФС, які впливають на питомий електроопір, енергію активації, фоточутливість і термоелектричні властивості ZnO і ZnO:In.

Ключові слова: Позаземне УФ випромінювання, Оксид цинку, ZnO:In, Імпульсне електроосадження, SILAR, Точковий дефект.

REFERENCES

1. J. Gröbner, I. Kröger, L. Egli, G. Hülsen, S. Riechelmann, P. Sperfeld, *Atmos. Meas. Tech.* **10**, 3375 (2017).
2. J. Zhao, G. Cai, L. Cui, A.S. Larbi, K.D. Tsavdaridis, *Polymers* **9**, 402 (2017).
3. M.P. Aleksandrova, I.N. Cholakova, G.K. Bodurov, G.D. Kolev, G.H. Dobrikov, *Int. J. Mater. Metall. Eng.* **6**, 1068 (2012).
4. L. Wallenhorst, L. Gurău, A. Gellerich, H. Militz, G. Ohms, W. Viöl, *Appl. Surf. Sci.* **434**, 1183 (2018).
5. J.J. Reinosa, P. Leret, C.M. Álvarez-Docio, A.del Campo, J.F. Fernández, *Boletín de la Sociedad Española de Cerámica y Vidrio* **55**, 55 (2016).
6. R. Karsthof, H. von Wenckstern, M. Grundmann, *J. Vac. Sci. Technol. B* **34**, 04J107 (2016).
7. N.P. Klochko, V.R. Kopach, I.I. Tyukhov, D.O. Zhadan, K.S. Klepikova, G.S. Khrypunov, S.I. Petrushenko, V.M. Lyubov, M.V. Kirichenko, S.V. Dukarov, A.L. Khrypunova, *Sol. Energ.* **164**, 149 (2018).
8. R. Khokhra, B. Bharti, H.-N. Lee, R. Kumar, *Sci. Report.* **7**, 15032 (2017).
9. V.R. Kopach, K.S. Klepikova, N.P. Klochko, I.I. Tyukhov, G.S. Khrypunov, V.E. Korsun, V.M. Lyubov, A.V. Kopach, R.V. Zaitsev, M.V. Kirichenko, *Sol. Energ.* **136**, 23 (2016).
10. N. Rastkari, A. Eslami, S. Nasseri, E. Piroti, A. Asadi, *Pol. J. Environ. Stud.* **26**, 785 (2017).
11. N.P. Klochko, K.S. Klepikova, V.R. Kopach, G.S. Khrypunov, Y.O. Myagchenko, E.E. Melnychuk, V.M. Lyubov, A.V. Kopach, *Semiconductors* **50**, 352 (2016).
12. S.Y. Park, K. Kim, K.-H. Lim, B.J. Kim, E. Lee, J.H. Cho, Y.S. Kim, *J. Mater. Chem. C* 1, 1383 (2013).
13. M. Chávez, H. Juárez, M. Pacio, X. Mathew, R.G.L. Chaltel, M. Zamora, O. Portillo, *Revista Mexicana de Física* **62**, 124 (2016).
14. A.K. Zak, W.H.A. Majid, M.E. Abrishami, R. Yousefi, *Solid State Sci.* **13**, 251 (2011).
15. D.K. Schroder, *Semiconductor material and device characterization* (New York: John Wiley & Sons, Inc.: 2006).
16. M. Smirnov, A.P. Rambu, C. Baban, G.I. Rusu, *J. Adv. Res. Phys.* **1**, 021011 (2010).
17. G. Singh, S.B. Shrivastava, D. Jain, S. Pandya, T. Shripathi, V. Ganesan, *Bull. Mater. Sci.* **33**, 581 (2010).
18. S. Dhara, P.K. Giri, *Rev. Nanosci. Nanotechnol.* **2**, 1 (2013).
19. F.A. Selim, M.H. Weber, D. Solodovnikov, K.G. Lynn, *Phys. Rev. Lett.* **99**, 085502 (2007).
20. L. Schmidt-Mende, J.L. MacManus-Driscoll, *Mater. Today* **10**, 40 (2007).
21. A.B. Djurišić, A.M.C. Ng, X.Y. Chen, *Prog. Quantum Electron.* **34**, 191 (2010).
22. F. Yi, Y. Huang, Z. Zhang, Q. Zhang, Y. Zhang, *Opt. Mater.* **35**, 1532 (2013).
23. O. Lupan, V. Cretu, V. Postica, M. Ahmadi, B.R. Cuenya, L. Chow, I. Tiginyanu, B. Viana, T. Pauporté, R. Adelung, *Sensor. Actuat. B* **223**, 893 (2016).
24. A. van Dijken, E.A. Meulenkamp, D. Vanmaekelbergh, A. Meijerink, *J. Lumin.* **90**, 123 (2000).
25. S.A. Studenikin, M. Cocivera, *J. Appl. Phys.* **91**, 5060 (2002).
26. P.M.R. Kumar, C.S. Kartha, K.P. Vijayakumar, T. Abe, Y. Kashiwaba, F. Singh, D.K. Avasthi, *Semicond. Sci. Technol.* **20**, 120 (2005).
27. A. Tubtimtae, M.-W. Lee, *Superlattice. Microstructure.* **52**, 987 (2012).
28. H. Morkoç, Ü. Özgür. *Zinc Oxide: Fundamentals, Materials and Device Technology* (Weinheim: WILEY-VCH Verlag GmbH & Co. KGaA: 2009).
29. A. González-Carrazco, M. Herrera-Zaldívar, U. Pal, *J. Nanosci. Nanotech.* **8**, 1 (2008).
30. K. Nakamura, *IOP Conf. Series: Mater. Sci. Eng.* **108**, 012040 (2016).